Mechanism-Guided Descriptor for Hydrogen Evolution Reaction in 2D Ordered Double Transition-Metal Carbide MXenes

Junmei Du, Yifan Yan, Xiumei Li, Jiao Chen, Chunsheng Guo, Yuanzheng Chen*, Hongyan Wang*

School of Physical Science and Technology, Key Laboratory of Advanced Technology of Materials, Southwest Jiaotong University, Chengdu, Sichuan 610031, China

** Email: cyz@swjtu.edu.cn (Y.C.);* hongyanw@swjtu.edu.cn(H.W.)*;*

The supporting information file includes:

1. Formation energies for 19 MXene precursor MAX phase candidates……...Table S1

2. Single point energy calculations for different configurations of MXenes…Table S2

3. The value of bond dissociation enthalpies (BDE) in M-O……Table S3

4. Lattice constants of MXenes……. Table S4

5. The calculated ΔG_H of $Cr_2TiC_2O_2$ in vacuum, with implicit solvent effect and explicit solvent effect……. Table S5

6. Gibbs free energy in vacuum and solvent environment…..……...Table S6

7. Convergence testing of k-Point mesh and energy cutoff.....Fig. S1

8. Calculated band structure…..…….....Fig. S2

9.Scailling relationships of d band center with ΔG_H……..……...…Fig. S3

10.The projected crystal orbital Hamilton population (pCOHP) of H-O bond…Fig. S4

11. The pDOS and pCOHP of hydrogen adsorption on $Mo_2TiC_2O_2$……...….Fig. S5

12. The diagram of pCOHP of H-O and O-M′ on other MXene……..Fig. S6

13.Analysis of regulation between ΔG_H and electronegativity of the inner transition metal, as well as the number of inner transition layers…….Fig. S7

14. Relationships between ΔG_H and descriptor δ of $M'_2M''N_2O_2$ system……....Fig. S8

15. The configuration of $Cr_2TiC_2O_2$ with explicit solvation …….….. Fig. S9

16.Phonopy spectrum and Ab initio molecular dynamic……Fig. S10

Pauli electronegativity formula…….…Equation S1

17. Supplementary references

Table S1. The thermodynamic competitors for 19 MAX phase candidates are selected from the Materials Project database, along with their calculated formation energies. Specially, the formation energy of the experimental synthetic $Mo_2Ti_2AlC_3$ is calculated to be 16.565 eV/atom.[1, 2] Thus, formation energies less than 20 eV/atom at 0 K is regarded stable. Notably, reference 3 reported that $W_2Hf_2AlC_3$ is unstable based on formation energy calculations.[3, 4] In contrast, our findings suggest that $W_2Hf_2SiC_3$ may be stable compared to competitors.

MAX	**Competitors**	$E_{formation}$ **(eV/atom)**
Cr_2TiAlC_2	TiAl, CrC	-0.494
Cr_2VAlC_2	$AlCr_2$, VC, C	1.283
W_2TiAlC_2	AlW_2C, TiC,	-0.500
Mo_2VAlC_2	AlC, MoC, VMo	-3.007
Mo_2TiAlC_2	TiAl, MoC	-1.873
Mo_2ZrAlC_2	ZrMo, MoC, AlC	-3.689
Mo_2HfAlC_2	HfMo, MoC, AlC	-3.831
Mo_2NbAlC_2	NbMo, MoC, AlC	-2.586
Mo_2TaAlC_2	TaMo, MoC, AlC	-2.709
$Nb_2Hf_2AlC_3$	HfNb, AlC_3	-14.383
$Cr_2Ti_2AlC_3$	Ti_2AlC, CrC	-0.436
$Cr_2V_2AlC_3$	AlV_2C, CrC	0.625
$Cr_2Ta_2AlC_3$	Ta_2AlC, CrC	-0.282
$W_2Ti_2AlC_3$	TiW, AlC_3	-14.528
$Mo_2Ti_2AlC_3$	TiMo, AlC_3	16.565
$Mo_2Zr_2AlC_3$	ZrMo, AlC_3	3.954
$Mo_2Hf_2AlC_3$	MoHf, AlC_3	5.291
$Mo_2Nb_2AlC_3$	NbMo, AlC_3	-12.493

$Mo_2Ta_2AlC_3$	TaMo, AlC_3	-12.819
$W_2Hf_2SiC_3$	HfW_2, HfSi,C	-19.921

Table S2. The energies of four unique configurations of O-terminated MXenes after geometric optimization.

MXenes	**hcp-fcc**	**fcc-hcp**	**fcc-fcc**	**hcp-hcp**
$Cr_2TiC_2O_2$	-62.29316887	-62.58999530	-62.57806371	**-62.79932329**
$Cr_2VC_2O_2$	-62.91888139	-62.65982005	-62.99283369	**-63.03072347**
$W_2TiC_2O_2$	-70.42501407	-70.42506373	-69.80046285	**-71.12732904**
$Mo_2VC_2O_2$	-67.22922395	-66.49722447	-65.88306397	**-67.22988186**
$Mo_2TiC_2O_2$	-66.73865261	-66.73878875	-66.15475182	**-67.35062443**
$Mo_2ZrC_2O_2$	-66.85718421	-66.87978266	-66.24968109	**-67.40379599**
$Mo_2HfC_2O_2$	-68.43626310	-68.34209335	-67.92651424	**-69.0124171**
$Mo_2NbC_2O_2$	-67.60385938	-67.72733877	-67.37521414	**-68.06066883**
$Mo_2TaC_2O_2$	-69.45909649	-69.47304364	-68.94471227	**-69.72906875**
$Nb_2Hf_2C_3O_2$	-90.63782585	-90.64447992	**-90.94965044**	-90.27246643
$Cr_2Ti_2C_3O_2$	-81.15490772	-81.15458795	**-81.28082960**	-81.21016333
$Cr_2V_2C_3O_2$	-79.72878967	-79.72889020	**-80.48541463**	-79.20834079
$Cr_2Ta_2C_3O_2$	-87.76774479	-87.76765430	**-88.36857801**	-87.09969920
$W_2Ti_2C_3O_2$	-89.40253520	-89.40227667	-88.79891700	**-90.05977445**
$Mo_2Ti_2C_3O_2$	-85.64097750	-85.64086701	-85.10330856	**-86.25980388**
$Mo_2Zr_2C_3O_2$	-86.56488878	-86.56494706	-86.23249742	**-86.95799804**
$Mo_2Hf_2C_3O_2$	-89.75590340	-89.75797703	-89.38242849	**-90.17013688**
$Mo_2Nb_2C_3O_2$	-88.05220668	-88.05227979	-87.78076802	**-88.49641118**
$Mo_2Ta_2C_3O_2$	-92.18208384	-92.18213071	-91.95617650	**-92.62988472**

Table S3. The value of bond dissociation enthalpies (BDE) in M-O.[5]

Bond	BDE (eV)	Bond	BDE (eV)
Cr-O	4.45	Nb-O	7.80
Mo-O	6.32	Ti-O	6.91
W-O	6.90	V-O	5.68
Hf-O	8.30		

Table S4. The lattice constant of MXenes.

MXene	a	b	c	alpha	beta	gamma
$Mo_2Zr_2C_3O_2$	6.16	6.16	24.85	90.00	90.04	120.00
$Mo_2Hf_2C_3O_2$	6.12	6.12	30.98	90.00	90.00	120.00
$Mo_2HfC_2O_2$	6.00	5.99	28.20	90.00	90.00	120.00
$Mo_2Nb_2C_3O_2$	6.01	6.01	24.92	90.00	90.02	120.00
$Mo_2NbC_2O_2$	5.90	5.91	27.02	90.00	90.00	120.00
$Mo_2Ta_2C_3O_2$	5.99	5.99	29.92	90.00	90.00	120.00
$Mo_2TaC_2O_2$	5.90	5.90	28.20	90.00	90.00	120.00
$Mo_2Ti_2C_3O_2$	5.90	5.90	24.92	90.00	90.02	120.00
$Mo_2TiC_2O_2$	5.85	5.85	27.88	90.00	90.00	120.00
$Mo_2VC_2O_2$	5.78	5.78	29.10	90.00	90.00	120.00
$Mo_2ZrC_2O_2$	6.01	6.01	27.29	90.00	90.06	120.00
$Cr_2Ta_2C_3O_2$	6.12	6.12	29.62	90.00	90.00	120.00
$Cr_2Ti_2C_3O_2$	5.96	5.96	28.45	90.00	90.00	120.00
$Cr_2TiC_2O_2$	5.61	5.61	26.99	90.00	90.00	120.00
$Cr_2V_2C_3O_2$	5.94	5.94	28.45	90.00	90.00	120.00
$Cr_2VC_2O_2$	5.52	5.52	28.95	90.05	90.00	120.00
$Nb_2Hf_2C_3O_2$	6.38	6.38	30.98	90.00	90.00	120.00
$W_2Ti_2C_3O_2$	5.91	5.91	29.92	90.00	90.00	120.00

$W_2TiC_2O_2$	5.87	5.87	26.37	90.04	90.54	120.00

Table S5. The calculated for slab energy of $Cr_2TiC_2O_2$, energy of adsorbed H on $Cr_2TiC_2O_2$, and the corresponding ΔG_H in Vacuum, with implicit solvent effect and explicit solvent effect.

$Cr_2TiC_2O_2$	**Slab Energy (eV)**	**Slab-H Energy (eV)**	**Slab-H ΔG (eV)**	**ΔG_{H^*} (eV)**
Vacuum	-249.51	-253.63	0.22	-0.49
Implicit	-249.51	-254.16	0.30	-0.94
Explicit	-303.41	-307.97	0.30	-0.86

Table S6. The Gibbs free energy results are calculated in vacuum and solvent environment.

MXene	**ΔG_H (eV) (vacuum)**	**ΔG_H (ev) (implicit solvation)**
$Mo_2TiC_2O_2$	0.175	-0.388
$Mo_2VC_2O_2$	-0.028	-0.592
$Mo_2NbC_2O_2$	-0.054	-0.610
$Mo_2HfC_2O_2$	0.660	-0.678
$Mo_2Ta_2C_3O_2$	0.144	-0.527
$Mo_2Zr_2C_3O_2$	0.189	-0.376
$Mo_2Ti_2C_3O_2$	0.125	-0.500
$Mo_2Nb_2C_3O_2$	-0.004	-0.117
$Mo_2Hf_2C_3O_2$	0.358	-0.155
$Ti_2MnC_2O_2$	-0.10	-0.590
$Ti_2TaC_2O_2$	-0.189	-0.492
$Ti_2Nb_2C_3O_2$	-0.079	-0.478
$W_2TiC_2O_2$	0.525	-0.482
$W_2ZrC_2O_2$	0.766	0.237
$W_2Zr_2C_3O_2$	0.503	-0.070

$W_2Hf_2C_3O_2$	0.584	-0.033
$Nb_2Ta_2C_3O_2$	0.152	-0.333

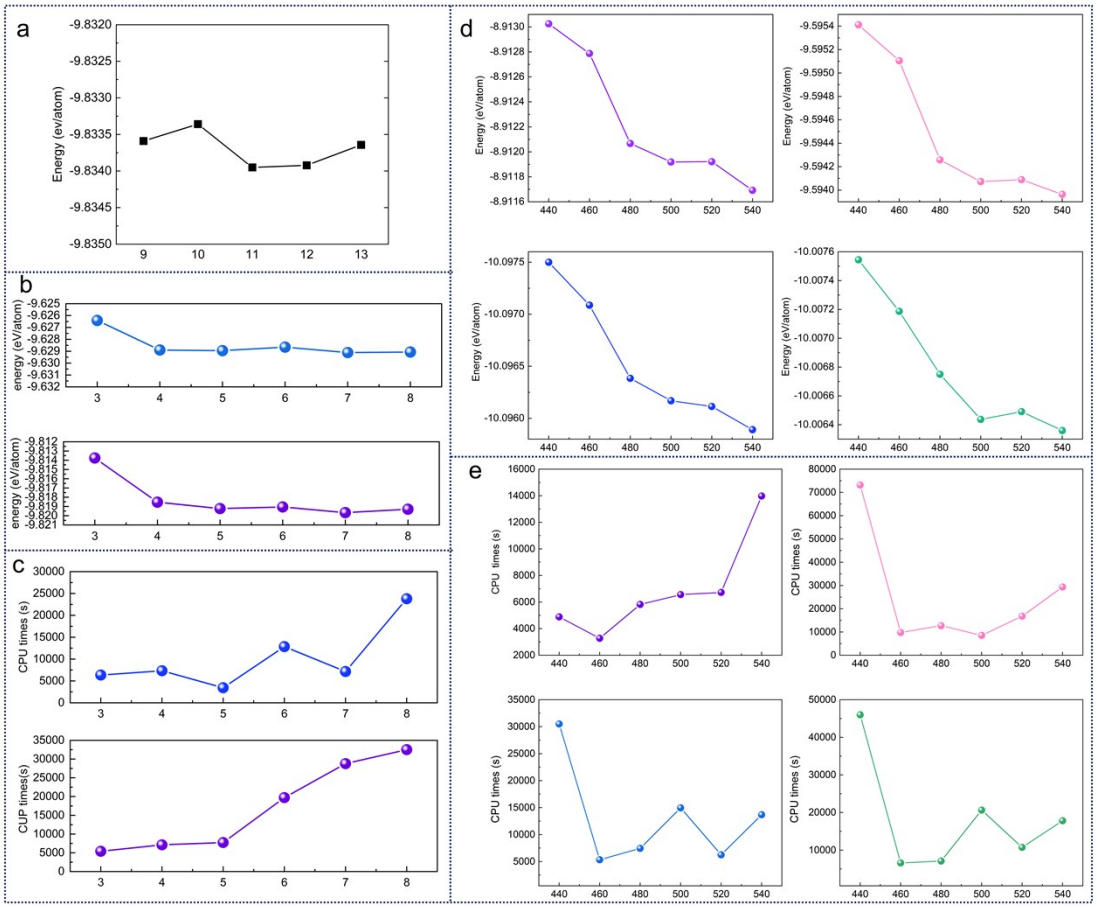

Fig. S1 The convergence tests of k-point mesh and energy cutoff for the computational accuracy on single or supercell MXenes. (a) The energy convergence tests of k-point mesh from 9×9×1 to 13×13×1 are performed to test the calculation accuracy on single cell, take $Mo_2Nb_2C_3O_2$ as example. (b)-(c) Energy convergence and computational cost (CPU time) tests are systematically conducted by varying the k-point mesh from 3×3×1 to 8×8×1 in a 2×2×1 supercell, respectively. Two representative systems are selected: $Cr_2Ta_2C_3O_2$ (top panel) and $Mo_2ZrC_2O_2$ (bottom panel), as shown in the respective panels. (d)-(e) Energy convergence and computational cost (CPU time) tests are systematically conducted by varying energy cutoff from 440 to 540 in a 2×2×1 supercell, respectively. Four representative systems are selected: $Cr_2TiC_2O_2$ (upper-left

panel), $Mo_2TiC_2O_2$ (upper-right panel), $Ti_2Ta_2C_3O_2$ (bottom-left panel) and $W_2Ti_2C_3O_2$ (bottom- right panel) as shown in the respective panels.

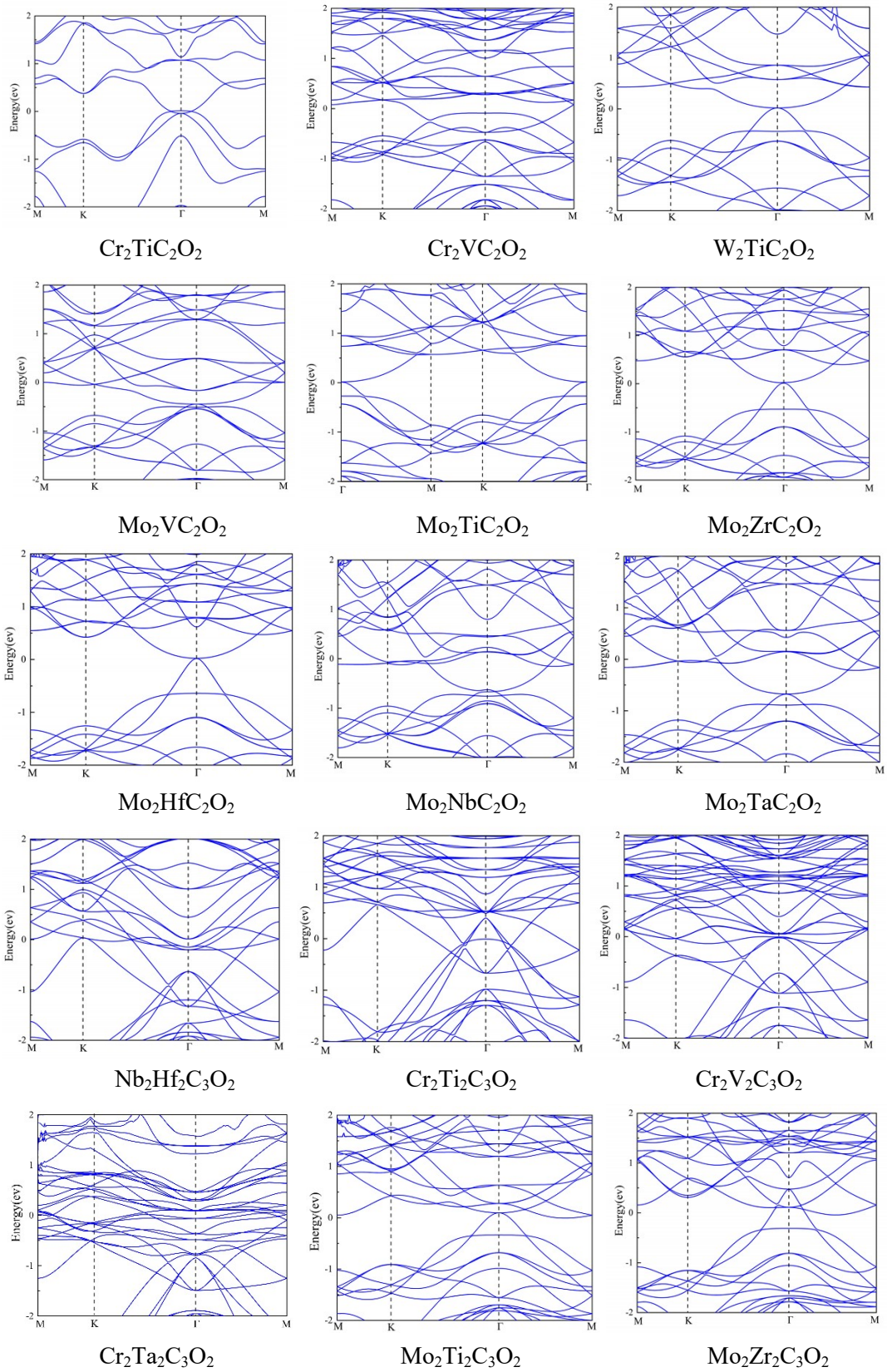

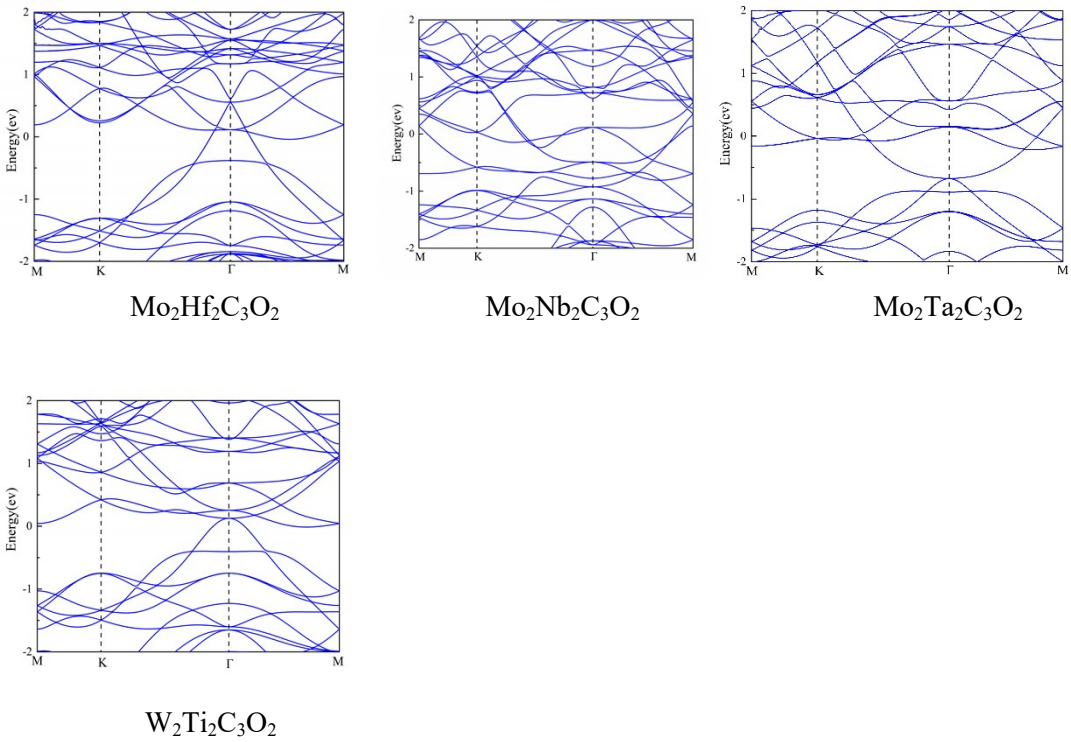

Fig. S2 Calculated band structures of 19 transition ordered double MXenes.

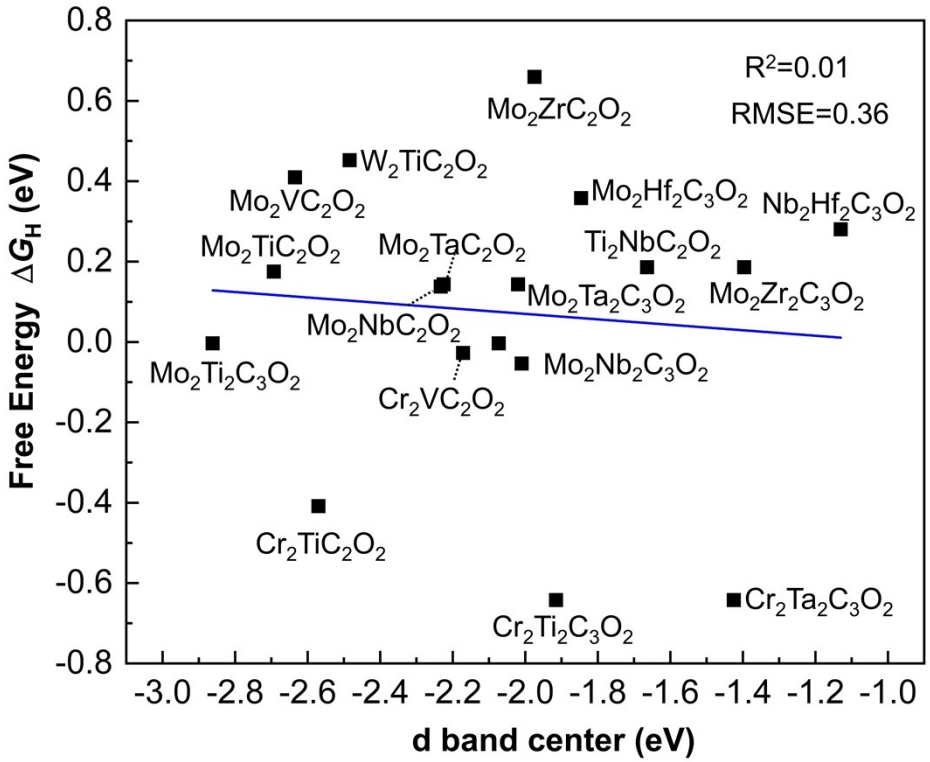

Fig. S3 Relationships between ΔG_H and descriptors of d-band center of the first-layer transition metal among different MXenes system.

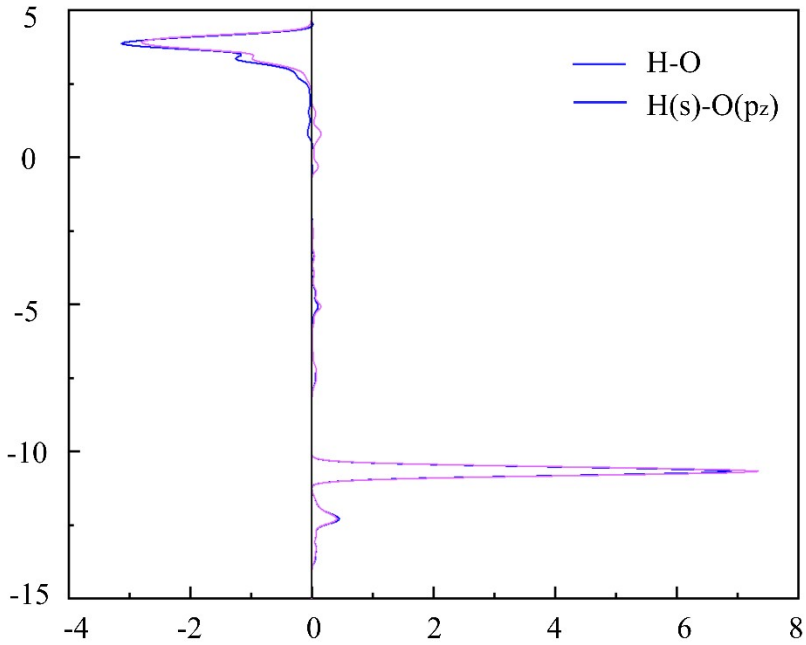

Fig. S4 The projected crystal orbital Hamilton population (pCOHP) of H-O bond when H adsorption on $Mo_2Ti_2C_3O_2$ as example.

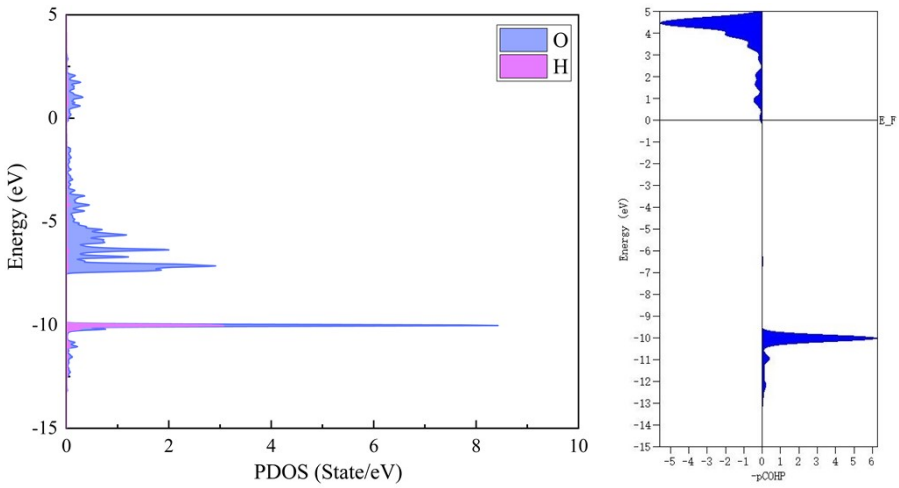

Fig. S5 The projected density of states (pDOS) and pCOHP with H adsorption on $Mo_2Ti_2C_3O_2$ as example.

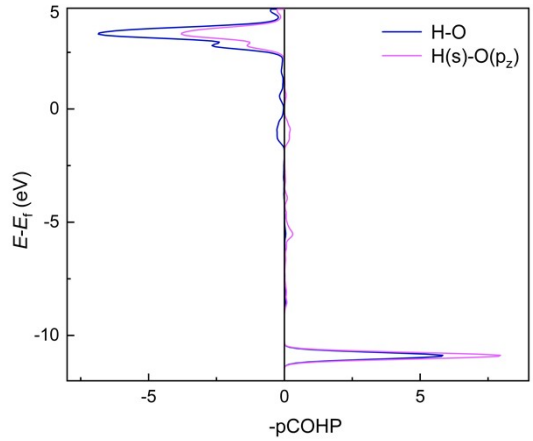

$Cr_2TiC_2O_2$

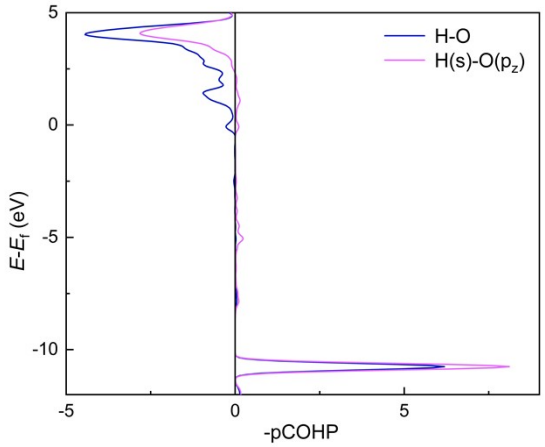

$W_2TiC_2O_2$

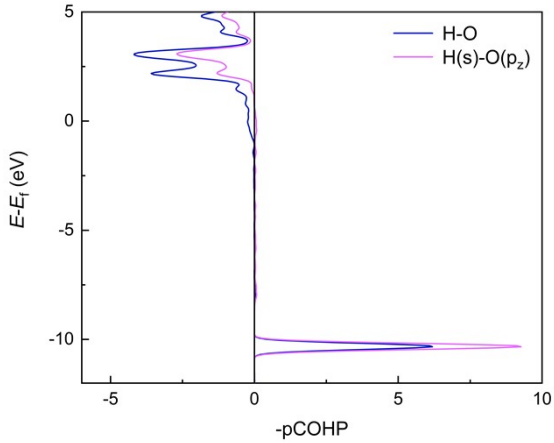

$Ti_2NbC_2O_2$

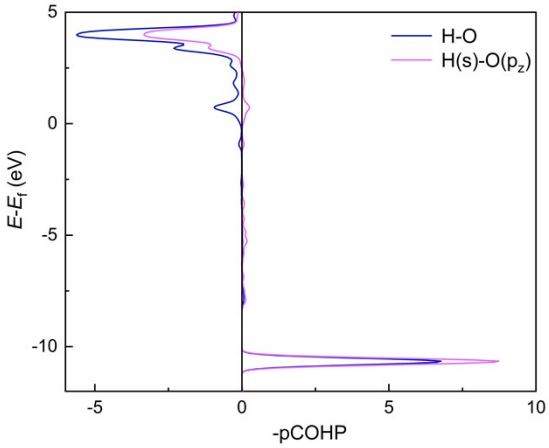

$Mo_2VC_2O_2$

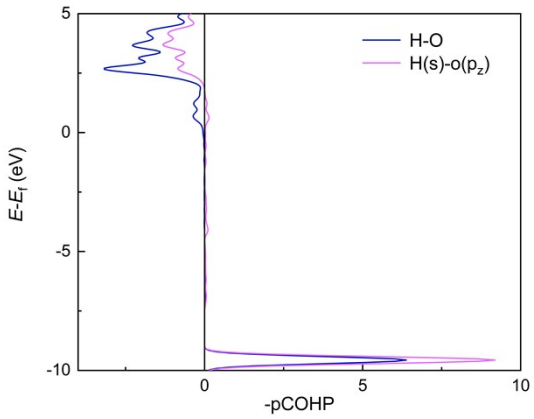

$Nb_2Hf_2C_3O_2$

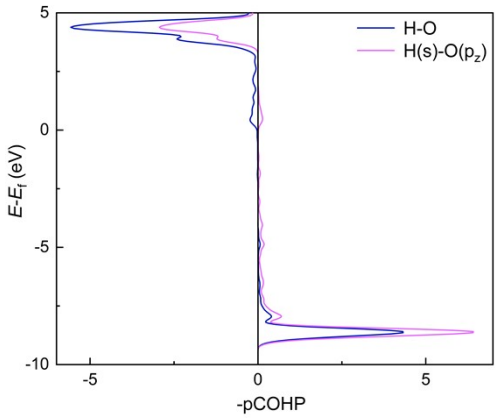

$V_2Ta_2C_3O_2$

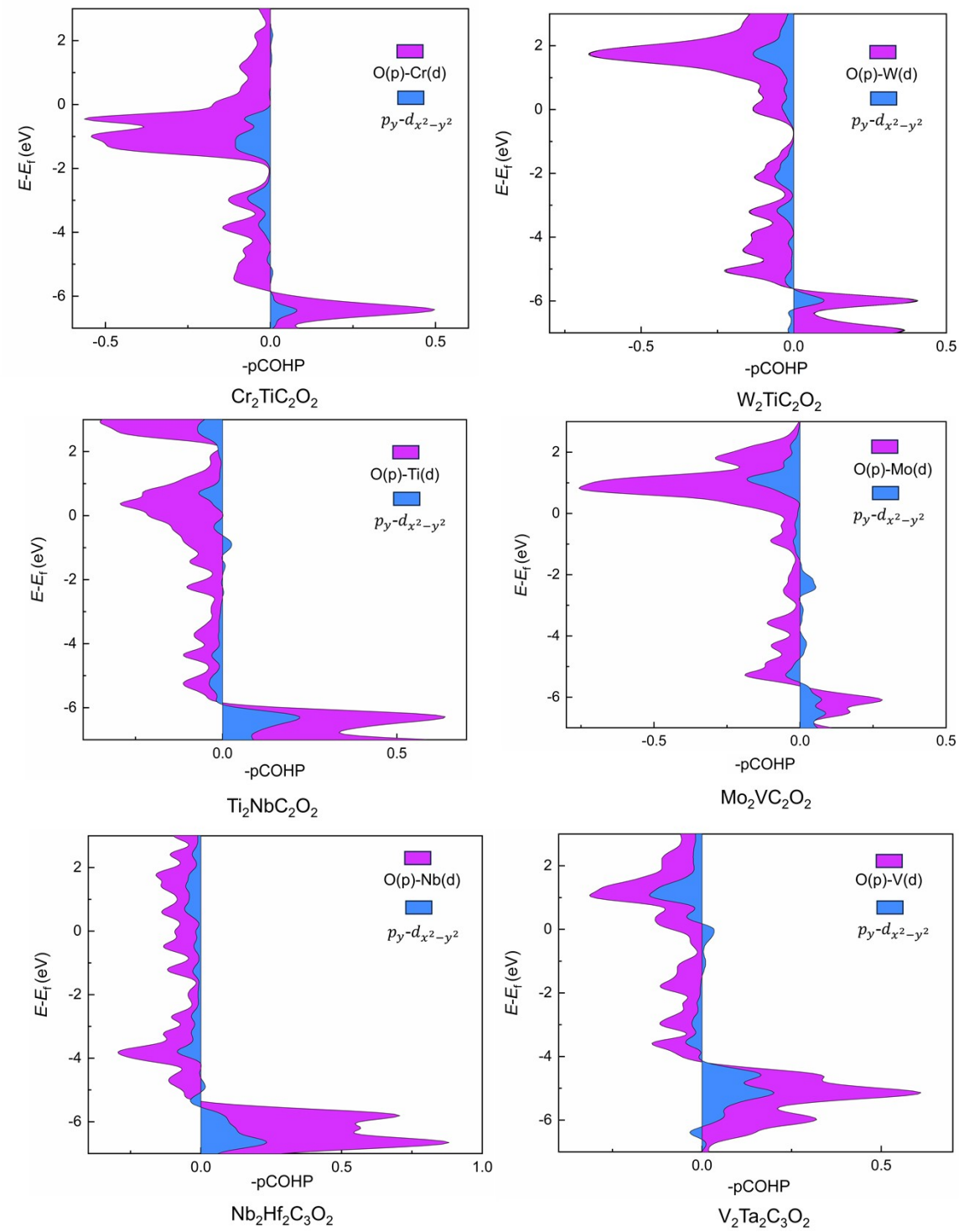

Fig. S6 The diagram of pCOHP plots of H-O, H(1s)-O(p_z), O(p)-M′(d) and O(p_y)-M′ ($d_{x^2-y^2}$) for MXenes, including $Cr_2TiC_2O_2$, $W_2TiC_2O_2$, $Ti_2NbC_2O_2$, $Mo_2VC_2O_2$, $Nb_2Hf_2C_3O_2$, and $V_2Ta_2C_3O_2$, respectively.

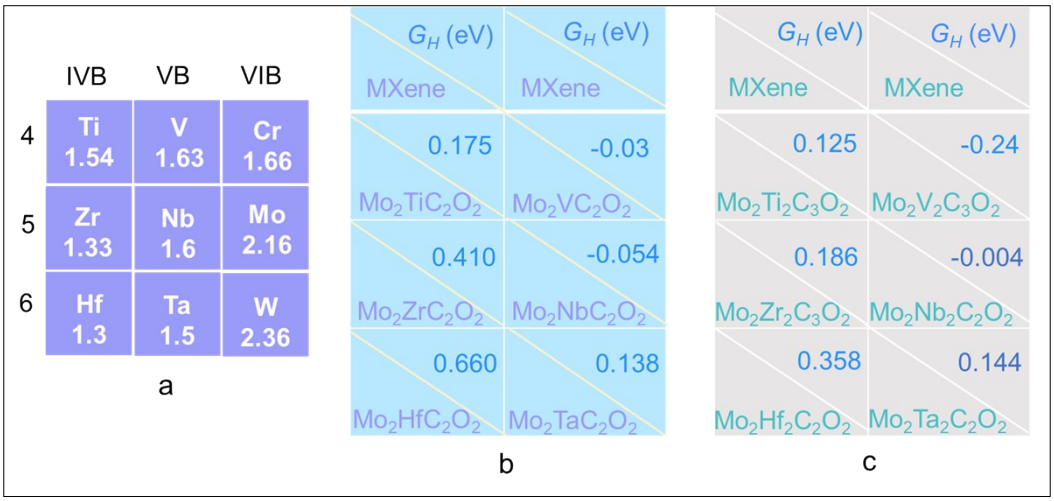

Fig. S7 Regulation between ΔG_H and electronegativity of the inner transition metal, and ΔG_H with the number of inner transition layers. a) The electronegativity values of elements in the third to sixth period and groups IVB-VIB, corresponding to the transition metals in $M_2MC_2O_2$ and $M_2M_2C_3O_2$, are illustrated. b-c) The overall trend of calculated ΔG_H decreases with increasing electronegativity of the inner transition metal based on Mo-based $M_2MC_2O_2$ and $M_2M_2C_3O_2$, respectively. Only a few materials, such as $Mo_2TaC_2O_2$ and $Mo_2Ta_2C_3O_2$, deviate from this trend. Additionally, the overall trend of calculated ΔG_H decreases with the increased number of inner transition layers, exception for $Mo_2Ta_2C_3O_2$.

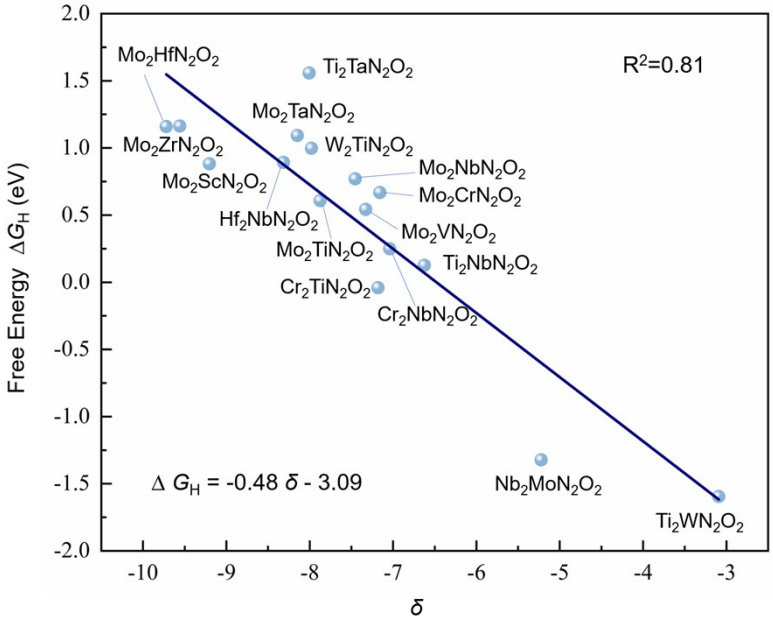

Fig. S8 Relationships between ΔG_H and descriptor δ of $M'_2M''N_2O_2$ system.

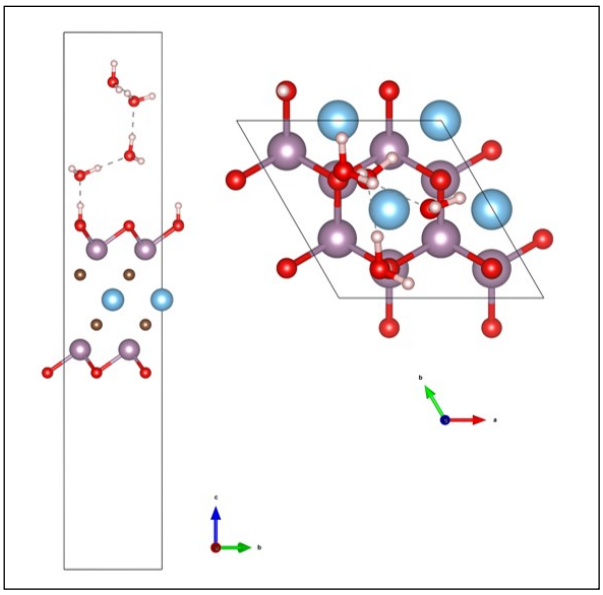

Fig. S9 The configuration of $Cr_2TiC_2O_2$ with explicit solvation by using four H_2O molecules.

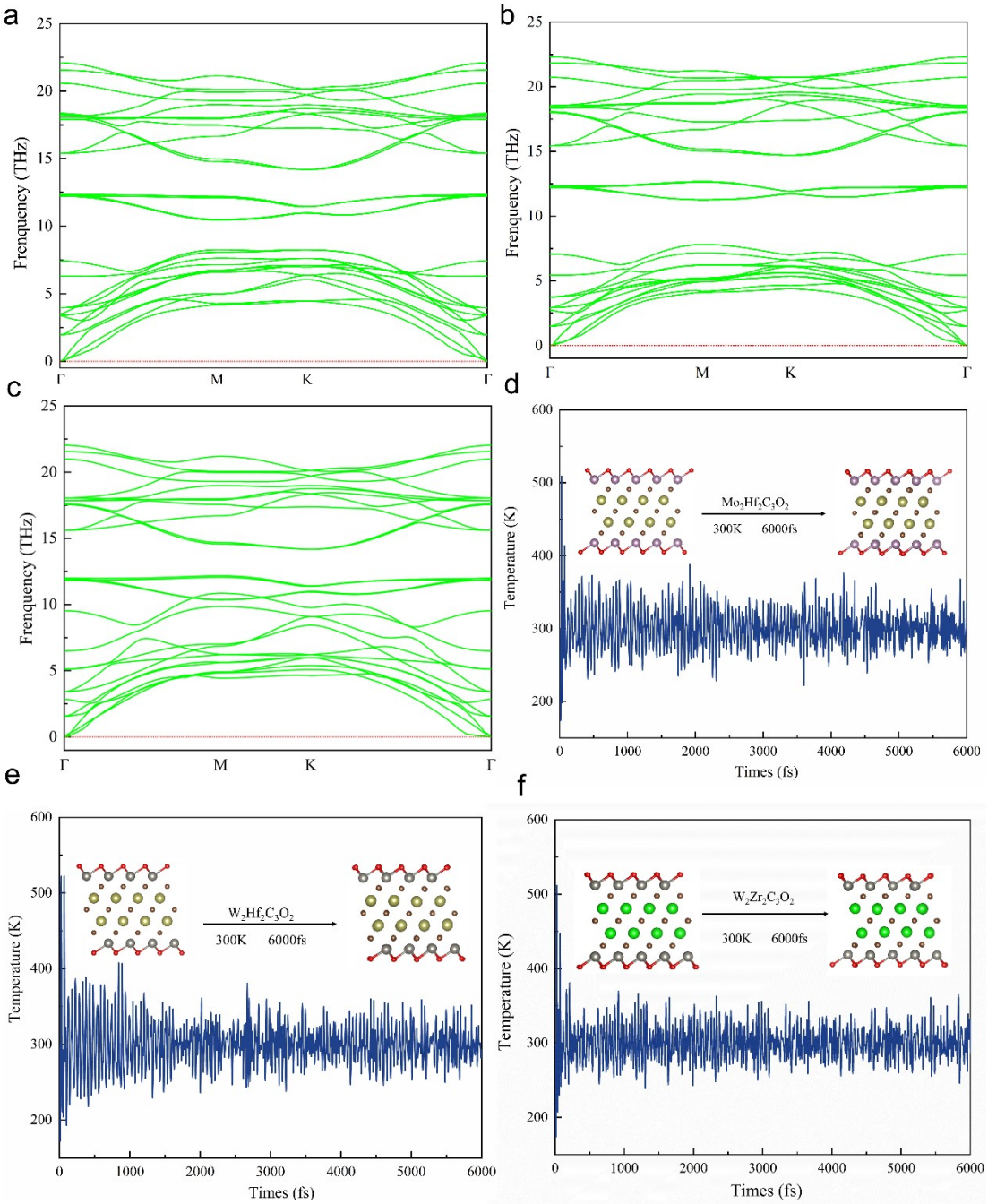

Fig. S10 a-c) Phonopy spectrum of $Mo_2Hf_2C_3O_2$, $W_2Hf_2C_3O_2$ and $W_2Zr_2C_3O_2$, respectively. d-f）Ab initio molecular dynamic of $Mo_2Hf_2C_3O_2$, $W_2Hf_2C_3O_2$ and $W_2Zr_2C_3O_2$, respectively.

Equation S1. Pauli electronegativity formula as follows,[6, 7]

$$|x_A - x_B| = eV^{-1/2}\sqrt{E_d(AB) - \frac{E_d(AA) + E_d(BB)}{2}}$$

References:

1. J. Yang, H. Zou, J. Chen, Y. Wen, Y. Fan, Y. Liu, L. Xiong and X. Li, Reactive synthesis of porous $Mo_2Ti_2AlC_3$ ceramic and its basic application properties, *Ceram. Int*, 2022, **48**, 9205-9217.
2. S. Fu, Y. Liu, H. Zhang, S. Grasso and C. Hu, Synthesis and characterization of high purity $Mo_2Ti_2AlC_3$ ceramic, *J. Alloys Compd.*, 2020, **815**, 152485.
3. M. Dahlqvist and J. Rosen, Predictive theoretical screening of phase stability for chemical order and disorder in quaternary 312 and 413 MAX phases, *Nanoscale*, 2020, **12**, 785-794.
4. A. Jain, S. P. Ong, G. Hautier, W. Chen, W. D. Richards, S. Dacek, S. Cholia, D. Gunter, D. Skinner, G. Ceder and K. A. Persson, Commentary: The Materials Project: A materials genome approach to accelerating materials innovation, *APL Materials*, 2013, **1**, 011002.
5. A. L. Allred, Electronegativity values from thermochemical data, *J. Manuf. Process.*, 1961, **17**, 215-221.
6. S. Trasatti, Electronegativity, work function, and heat of adsorption of hydrogen on metals, *J. Chem. Soc., Faraday Trans. 1*, 1972, **68**, 229-236.
7. J. A. Dean, LANGE'S HANDBOOK OF CHEMISTRY, *J. inorg. nucl. chem*, 2010, **5**, 687-688.